Fatigue Crack Growth Behavior of Gas Metal Arc Welded AISI 409 Grade Ferritic Stainless Steel Joints

A.K. Lakshminarayanan, K. Shanmugam, and V. Balasubramanian

The effect of filler metals such as austenitic stainless steel, ferritic stainless steel, and duplex stainless steel on fatigue crack growth behavior of the gas metal arc welded ferritic stainless steel joints was investigated. Rolled plates of 4 mm thickness were used as the base material for preparing single 'V' butt welded joints. Center cracked tensile specimens were prepared to evaluate fatigue crack growth behavior. Servo hydraulic controlled fatigue testing machine with a capacity of 100 kN was used to evaluate the fatigue crack growth behavior of the welded joints. From this investigation, it was found that the joints fabricated by duplex stainless steel filler metal showed superior fatigue crack growth resistance compared to the joints fabricated by austenitic and ferritic stainless steel filler metals. Higher yield strength and relatively higher toughness may be the reasons for superior fatigue performance of the joints fabricated by duplex stainless steel filler metal.

1. Introduction

Ferritic stainless steels (FSS) are used in a less severe corrosive atmosphere for chemical processing equipment, furnace parts, heat exchangers, oil burner parts, petroleum refining equipment, protection tubes, recuperates, storage vessels, electrical appliances, solar water heaters, and household appliances (Ref 1). Due to the increasing use of fusion joining in such industrial applications, the welding metallurgy of FSS has drawn much attention recently. However, joining of FSS is faced with the problem of coarse grains in the weld zone and heat-affected zone of fusion welds and consequent low toughness and ductility due to the absence of phase transformation during which grain refinement can occur (Ref 2, 3). Excessive grain growth can be avoided, of course, by using lower welding heat inputs. It has also been suggested that nitride and carbide formers such as B, Al, V, and Zr can be added to FSS to suppress grain growth during welding (Ref 4).

Villafuerte and Kerr (Ref 5) attempted to weld FSS by gas tungsten arc welding (GTAW) process and observed that approximately for constant values of heat input per unit distance, the equiaxed grain fraction increased with welding speed, as long as sufficient titanium and aluminum were present to form nucleate for the second phase. In a later study by Villafuerte et al. (Ref 6), the tin quenching of GTA welds of commercial FSS had shown direct evidence of heterogeneous nucleation of equiaxed grains on tin particles ahead of advancing columnar interfaces. A technique was developed for quenching of moving weld puddles, using liquid tin. The technique was used to characterize solidification modes during GTA weld solidification of austenitic and FSS. Quenching of the pool was obtained by pouring liquid tin at 350 °C through a stainless steel funnel inserted into an auxiliary shielding chamber. The power supply was turned off on contact of the liquid tin with the surface of the weld puddle, extinguishing the arc. The relatively cold liquid tin was effective in rapidly cooling the steel close to the advancing solid-liquid interface. However, the addition of titanium alone did not lead to the formation of equiaxed grains, despite an increased tendency for branching and the protrusion of some primary dendrite stalks ahead of others.

Mohandas et al. (Ref 7) made a comparative evaluation of gas tungsten and shielded metal arc welds of AISI 430 FSS and found that the greater ductility and strength of gas tungsten arc welds as compared to those of shielded metal arc welds can be attributed to the equiaxed morphology of the fusion-zone grains in the gas tungsten arc welds, and also to inert gas shielding. Meyers and Toit (Ref 8) investigated the impact properties of 11-12% chromium steels and found that carbon and nitrogen affect the impact properties of the heat-affected zone in these steels. Silva et al. (Ref 9) investigated the microstructural characteristics of the HAZ in AISI 444 FSS and reported that needle-like Laves phase precipitation occurred in the HAZ, near the partially melted zone, and other secondary phases such as χ and σ, as well as nitride, carbide, and carbonitride precipitates, were also observed.

Most of the reported literature focused on the effect of welding processes on the fusion zone microstructure and tensile and impact properties. But published information on fatigue crack growth behavior of FSS is not available. Hence, the present investigation was carried out to understand the effect of filler metals on fatigue crack growth behavior of gas metal arc welded (GMAW) FSS joints.

A.K. Lakshminarayanan, K. Shanmugam, and **V. Balasubramanian**, Department of Manufacturing Engineering, Centre for Materials Joining & Research (CEMAJOR), Annamalai University, Annamalai Nagar 608 002, Tamil Nadu, India. Contact e-mail: visvabalu@ yahoo.com.

2. Experimental

Rolled plates of 4 mm thickness AISI 409M grade FSS were cut into the required dimension (300 × 150 mm) by plasma cutting. The chemical composition of the base metal is presented in Table 1. The initial joint configuration was obtained by securing the plates in position using tack welding. Single 'V' butt joints were fabricated using GMAW process with austenitic stainless steel (ASS), FSS, and duplex stainless steel (DSS) filler metals. Single pass welding procedure was used to fabricate the joints. Necessary care was taken to avoid joint distortion and the joints were made by applying clamping devices. The welding conditions and process parameters used to fabricate the joints are given in Table 2. The soundness of the welded joints was checked using ultrasonic testing.

The welded joints were sliced using power hacksaw and then machined to the required dimensions for preparing tensile, impact, and fatigue test specimens as shown in Fig. 1. Tensile test was conducted in a 100 kN, electro-mechanical controlled Universal Testing Machine (Make: FIE-BLUE STAR, India; Model: UNITEK-94100). ASTM E8M-04 guidelines were followed for preparing and testing the tensile specimens. Since the plate thickness is small, subsize impact specimens were prepared. Impact test was conducted at room temperature using pendulum type impact testing machine (Make: ENKAY, India) with a maximum capacity of 30 J. ASTM E23-04 specifications were followed for preparing and testing the specimens.

For center cracked tensile (CCT) specimen, the sharp notch (5 mm length and 0.05 mm tip radius) was machined in the middle of the fusion zone region using the wire-cut electric discharge machining (WEDM) process. Procedures prescribed by the ASTM E647-04 (ASTM, 2004) standard were followed for the preparation of the specimens. Fatigue crack growth experiments were conducted using a 100 kN, servo hydraulic universal testing machine. A frequency of 20 Hz under constant amplitude loading ($R = 0$) was used for all fatigue tests. Before loading, the specimen surface near the notch was polished to facilitate fatigue crack growth measurement. A traveling microscope with an accuracy of 0.01 mm was used to monitor the crack length. The specimen was loaded at a particular stress level (range), and following crack initiation from the tip of the machined notch, its subsequent propagation into the weld metal was recorded from initiation to the complete failure of the specimen. Similar crack growth experiments were conducted on a number of specimens at various stress levels, and the experimental data were recorded.

Vicker's microhardness testing machine (Make: Shimadzu, Japan and Model: HMV-2T) was employed for measuring the hardness of the weld with 0.5 kg load. Microstructural examination was carried out using a light optical microscope (Make: MEJI, Japan; Model: MIL-7100) incorporated with an image analyzing software (Metal vision). The specimens for metallographic examination were sectioned to the required size from the joint comprising fusion zone region and were polished using different grades of emery papers. Final polishing was done using the diamond compound (1 μm particle size) in the disc polishing machine. The specimens were etched with 5 mL hydrochloric acid, 1 g picric acid, and 100 mL methanol applied for 10-15 s. The fractured surface of the fatigue tested specimens was analyzed using scanning electron microscope (SEM) (Make: JEOL, Japan; Model: 6410LV) at higher magnification to study the fracture morphology for establishing the nature of the fracture.

3. Results

3.1 Tensile and Impact Properties

Transverse tensile properties of the joints such as yield strength, tensile strength and percentage of elongation were evaluated and are presented in Table 3. In each condition, three specimens were tested, and the average of the three results is presented in Table 3. Of the three joints, GMADSS (fabricated by DSS filler metal) joint exhibited higher strength values, and the enhancement in strength value is approximately 15% compared to GMAASS (fabricated by ASS filler metal) joint and 7% compared to GMAFSS (fabricated by FSS filler metal) joint. Charpy impact toughness values of all the joints were evaluated and are presented in Table 3. Of the three joints, the GMAASS joint exhibited higher impact toughness values, and the enhancement in toughness value is approximately 27% compared to GMADSS joint and 72% compared to GMAFSS joint.

3.2 Hardness and Microstructure

During tensile test, all the welded joints fail invariably in the weld region, and hence microhardness was measured at the weld metal region of the joints and is presented in Table 3. The hardness of the GMAASS and GMAFSS joints in the weld metal region is 330 VHN and 350 VHN, respectively. However, the hardness of the GMADSS joints in the weld metal region is 370 VHN, which is relatively higher compared to GMAASS and GMAFSS joints. The microstructure of the

Table 2 Welding conditions and process parameters

Welding machine	Lincoln (Precision Tig 375), USA
Polarity	DCEP
Arc voltage, V	30
Welding current, A	120
Welding speed, mm/s	5
Heat input, J/mm	720
Electrode diameter, mm	1.6
Shielding gas	Argon (99.99%)
Shielding gas flow rate, L/min	14

Table 1 Chemical composition of base metal and weld metals (wt.%)

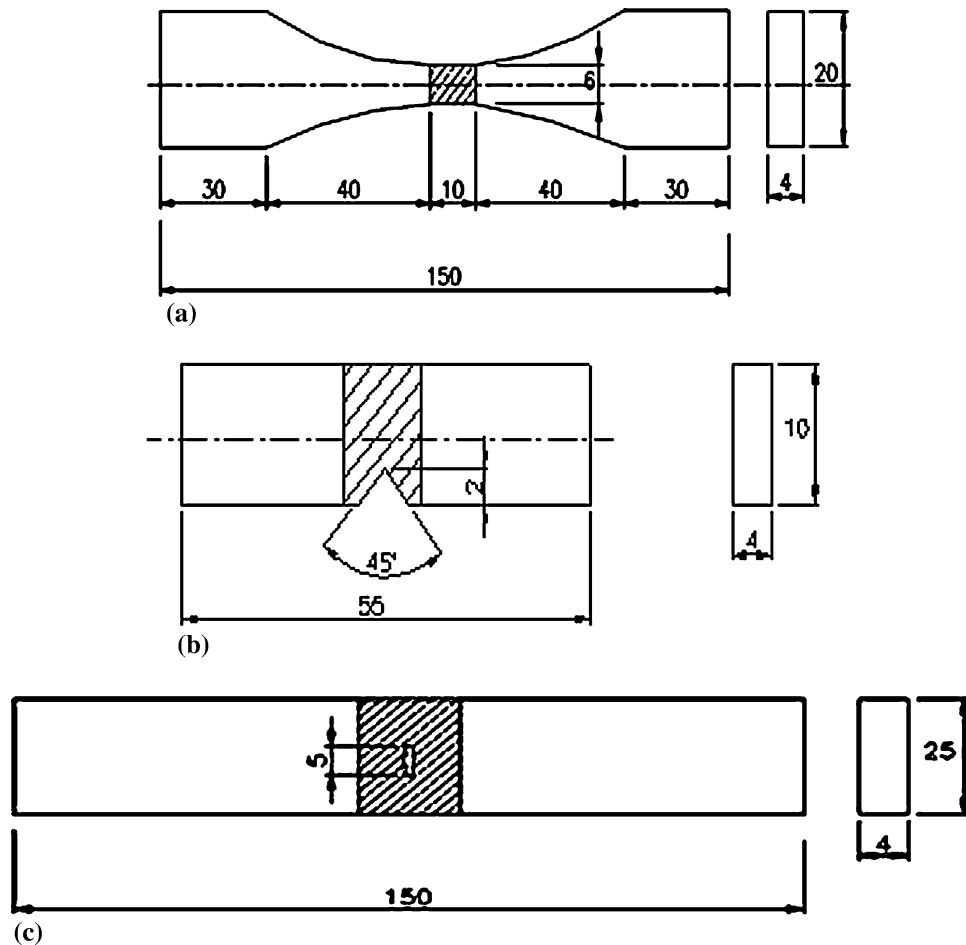| Material	C	Mn	P	S	Si	Cr	Ni	Ti	Mo	Cu	Fe
Base metal (AISI 409M)	0.080	1.10	0.030	0.010	0.40	10.90	0.39	0.004	…	…	Bal.
GMAASS (AWS ER 308L)	0.021	0.82	0.018	0.015	0.67	19.00	11.0	…	0.01	0.1	Bal.
GMAFSS (AWS ER 430)	0.030	0.70	0.017	0.014	0.60	17.00	0.40	…	…	…	Bal.
GMADSS (AWS ER 2209)	0.012	0.80	0.018	0.016	0.80	22.00	9.00	…	3.00	…	Bal.

Fig. 1 Dimensions of tensile, impact, and fatigue specimens. (a) Unnotched tensile specimen, (b) subsize impact specimen, and (c) center cracked tensile (CCT) specimen for fatigue crack growth test

Table 3 Tensile, hardness, and impact properties of base metal and welded joints

Joint	Yield strength, MPa	Tensile strength, MPa	Elongation, %	Hardness (VHN) at 0.5 kg load	Impact toughness, J
BM	359	524	12	430	22
GMAASS	185	230	8.65	250	21
GMAFSS	215	250	5.56	375	5
GMADSS	225	270	7.25	300	16

joints was examined at different locations but the optical micrographs taken at weld metal (WM) region alone are displayed in Fig. 2. The joints fabricated by ASS filler metals primarily contain solidified dendritic structure of austenite (Fig. 2b) and the joints fabricated by FSS filler metals contain solidified ferritic grains (Fig. 2c), whereas the joints fabricated by DSS filler metals contain solidified austenitic structure in the ferrite matrix (Fig. 2d).

3.3 Fatigue Crack Growth Behavior

The fatigue crack growth experiments were conducted at five different stress levels ($\Delta\sigma$) of 75, 100, 125, 150, and 175 MPa under constant amplitude loading conditions ($R = 0$). The measured variation in crack length (2a) and the corresponding number of cycles (N) endured under the action of particular applied stress range were recorded for all the joints. The fracture mechanics based Paris Power equation, given below, was used to analyze the experimental results.

$$\frac{\mathrm{d}a}{\mathrm{d}N} = C \times (\Delta K)^m$$

where $\mathrm{d}a/\mathrm{d}N$ is the crack growth rate, ΔK is the stress intensity factor (SIF) range, and C and m are constants. The SIF value was calculated for different values of growing fatigue crack length '2a' using the following expression (Ref 10):

$$(\Delta K) = \phi \times (\Delta\sigma) \times \sqrt{\pi a}$$

However, the geometry factor for the CCT specimen was calculated using the expression given below (Ref 11):

$$\phi = \sqrt{\{(W/\pi a) \cdot \tan(\pi a/W)\}}$$

The crack growth rate $\mathrm{d}a/\mathrm{d}N$ for the propagation stage was calculated for the steady-state growth regime, at different intervals of crack length increment, against the associated number of cycles to propagation. The relationship between SIF range and the corresponding crack growth rate in terms
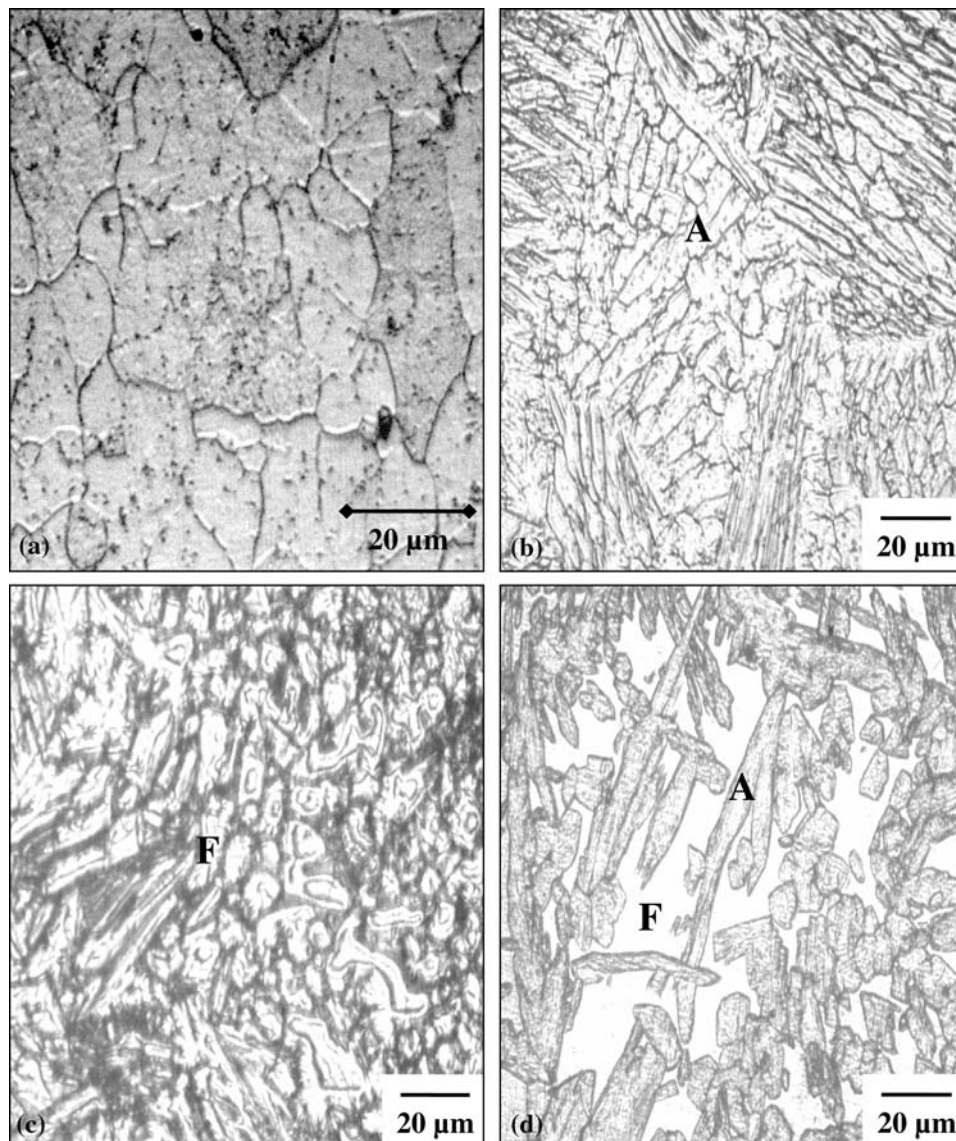
Fig. 2 Optical micrographs of base metal and weld metal region. (a) Base metal, (b) GMAASS, (c) GMAFSS, and (d) GMADSS. F, ferrite; A, austenite

of best fit lines is shown in Fig. 3 for all the joints. The data points plotted in the graph mostly correspond to the second stage of Paris sigmoidal relationship (10^{-6} to 10^{-3} mm/cycle). The exponent m, which is the slope of the line on log-log plot, and the intercept C of the line have been determined and are presented in Table 4.

Normally, in the case of steels, the threshold SIF (ΔK_{th}) value is obtained for a crack growth rate of 10^{-8} mm/cycle. Due to the specimen configuration and loading conditions, crack propagation rates in the region of 10^{-8} mm/cycle could not be obtained. Hence the SIF value obtained at a crack growth rate of 10^{-6} mm/cycle was taken as ΔK_{th} for comparison purpose. This value cannot be considered as design value.

Similarly, when the crack growth rate was around 10^{-3} mm/cycle, unstable crack growth occurred (the curve became parallel to the Y-axis) and the corresponding ΔK value was taken as critical (ΔK_{cr}). The value was not at fracture, and it is a transition point at which steady-state crack growth changes into

unsteady state. The fatigue crack growth (fracture mechanics) parameters of all the joints are compared in Table 4.

It is also advantageous to plot the standard S-N curve for the test conditions, which will indicate the trend and also be useful for design purposes. Figure 4 shows the relationship between stress range (S) and the number of cycles to failure (N) on a log-log plot for all the joints. The stress corresponding to 2×10^6 cycles is taken as an indication of the endurance limit (Ref 10), and these values are determined for all the joint combinations and are presented in Table 4.

The fatigue crack initiation (FCI) life, N_i, is evaluated experimentally using the crack "initiation criteria." The initiation criterion is assumed to be the number of cycles required for a crack to grow to an excess of 0.5 mm length from its original (initial) length, at the earlier crack growth stage under particular stress level. This is because, at this stage, the crack is expected to attain more regular and stable front shape. Similar criteria were adopted by other investigators

also (Ref 11, 12). Figure 5 shows the relationship that exists between applied stress range (S) and the crack initiation life (N_i) for all the joints. Each endurance line can be represented by a Basquin-type equation, in general form, as expressed below:

$$N_i = A \times (\Delta\sigma)^{-n}$$

where A and n are constants (n is the slope of the line and A is the intercept of the line) and their values are evaluated and presented in Table 4.

3.4 Fracture Surface

The fatigue fracture surface appearance corresponding to crack initiation, crack propagation, and the final failure (FF) regions of the joints (stress level of 100 MPa alone), as observed under the SEM, are displayed in Fig. 6-8. In FCI regions (within 1 mm from tip of machined notch), few crack initiations sites were observed and this suggests that the fatigue cracks have initiated from multiple crack initiation sites. The number of crack initiation sites is relatively more in the GMAFSS joint (Fig. 6b) compared to GMAASS (Fig. 6a) and GMADSS (Fig. 6c) joints and is evident from the FCI regions of SEM fractographs.

In fatigue crack propagation (FCP) region, where steady-state crack growth occurs, features such as beach markings (Fig. 7a), peaks and valleys produced by rubbing actions (Fig. 7b), micron level striations (Fig. 7c) were observed. These are the indications for steady-state crack growth, which depends on the material properties.
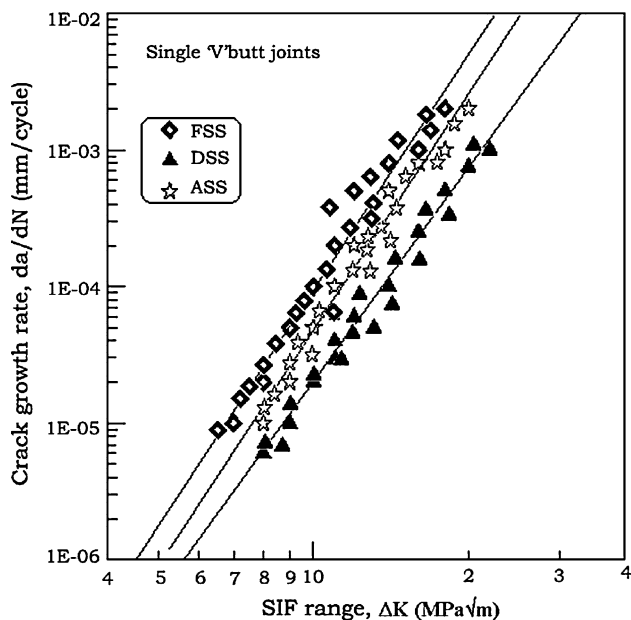
From the fractographs of FF region, it is observed that the tear dimples are elongated along the loading direction, and this is mainly because of the limit load condition at the time of
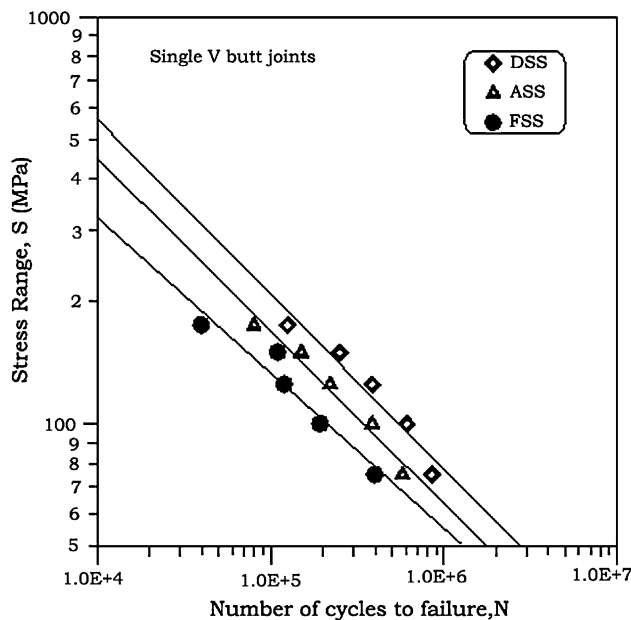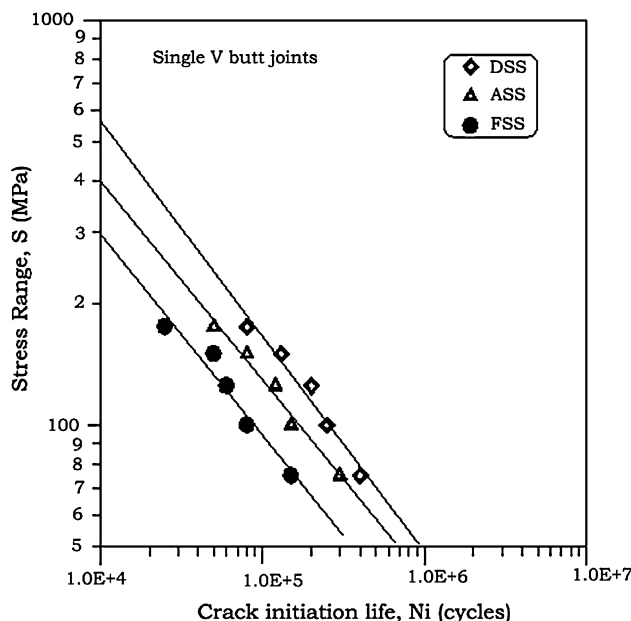

Fig. 4 *S-N* curves

Fig. 3 Relationship between FCGR and SIF range

Fig. 5 Relationship between stress range and fatigue crack initiation life

Table 4 Fatigue properties of ferritic stainless steel joints

Joints	m	C	n	A	ΔK_{th}, MPa√m	ΔK_{cr}, MPa√m	$\Delta\sigma_e$, MPa
GMAASS	5.45	1.56×10^{-10}	2.12	8.7×10^{10}	5.0	18	50
GMAFSS	5.73	1.72×10^{-10}	2.46	1.2×10^{11}	4.5	15	40
GMADSS	5.19	1.28×10^{-10}	1.85	5.6×10^{10}	5.5	21	60

Fig. 6 SEM fractographs of FCI region. (a) GMAASS, (b) GMAFSS, and (c) GMADSS. I, crack initiation site

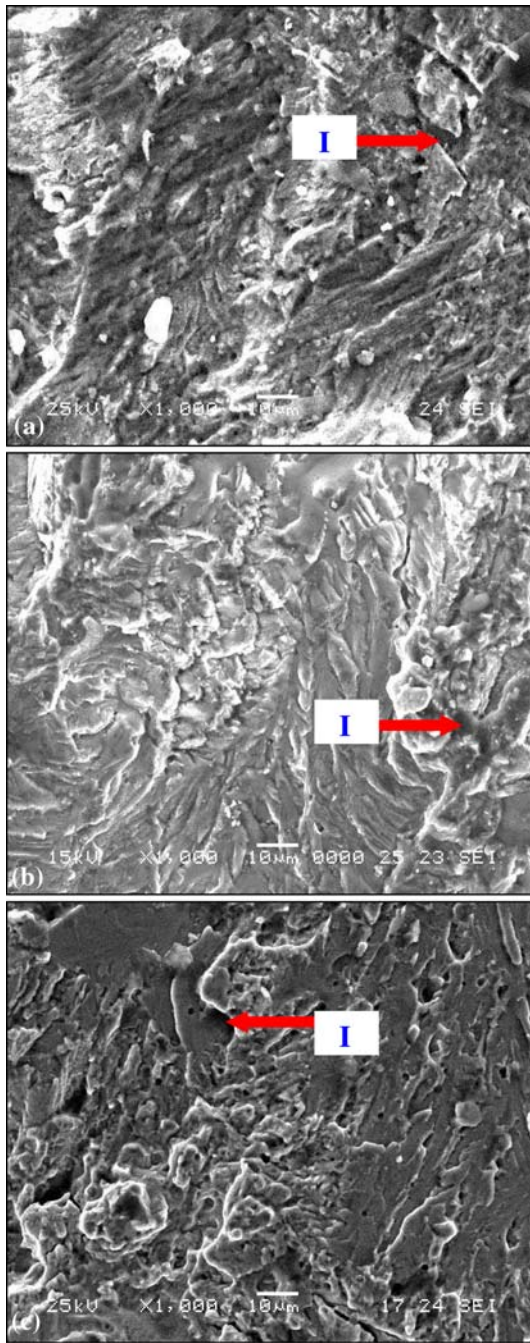**Fig. 7** SEM fractographs of FCP region. (a) GMAASS, (b) GMAFSS, and (c) GMADSS. S, striations

final fracture. Even though unstable crack growth occurs in the FF region, the final fracture is still in the ductile mode in the case of GMAASS (Fig. 8a) and GMADSS (Fig. 8c) joints and is evident from the presence of dimples. The final fracture of GMAFSS is in a brittle manner as shown in Fig. 8(b).

4. Discussion

The FCI behavior, FCP behavior, and fatigue life of FSS joints are influenced by the filler metals used. Of the three
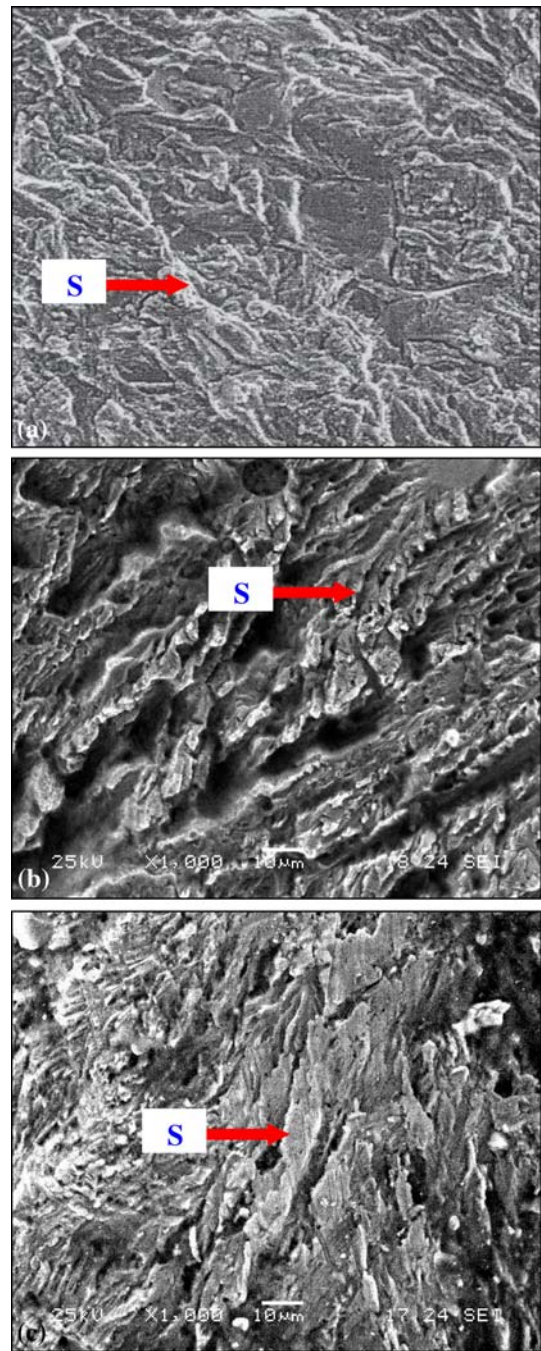
joints, GMADSS joints exhibit higher fatigue resistance than GMAASS and GMAFSS joints. In the CCT specimen, the notch is machined in the weld metal (WM) region of the joints by wire cut EDM (electric discharge machining) process to evaluate the crack growth behavior of the welded joints under fatigue loading. The fatigue crack initiates from the tip of the machined notch, and it grows in the weld metal region until FF takes place. Hence, the weld metal properties such as tensile strength, impact toughness, hardness, and microstructure will definitely influence the fatigue performance of the joints. The effect of these weld metal properties on fatigue performance is analyzed in detail in the following paragraphs.
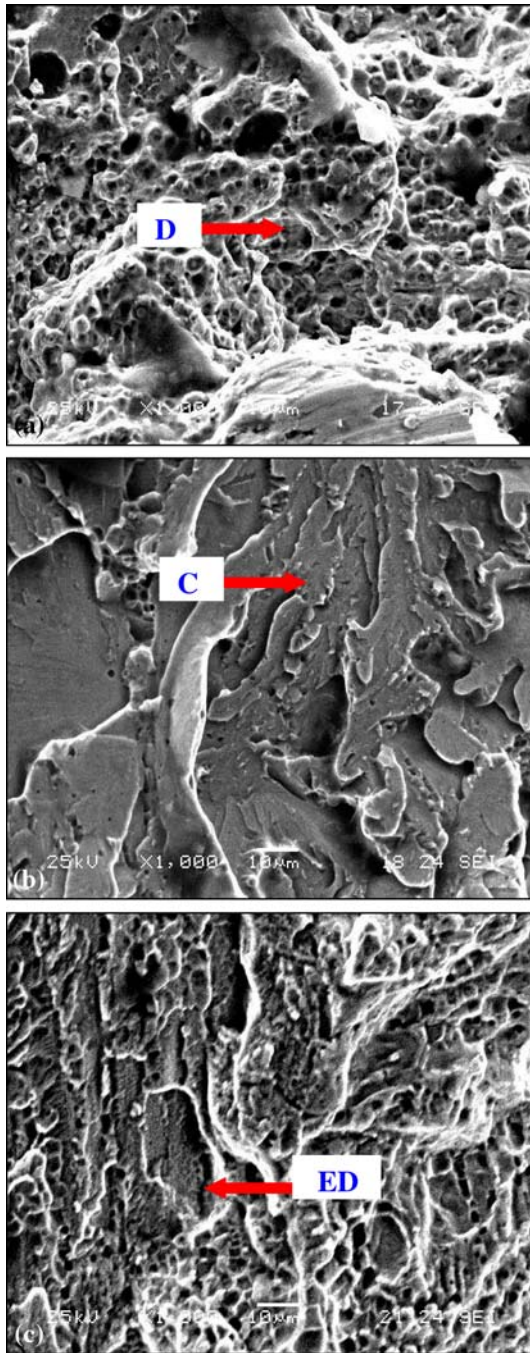
Fig. 8 SEM fractographs of FF region. (a) GMAASS, (b) GMAFSS, and (c) GMADSS. D, dimples; C, cleavage; ED, elongated dimples

The tensile properties (yield strength, tensile strength, and elongation) of GMADSS joints are superior as compared to their counterparts (Table 3). The variations in tensile, impact, and hardness properties of FSS joints are caused by the chemical composition of the weld metal and the microstructure of the weld metal.

The formation of fully austenitic structure in the weld metal region of GMAASS joint due to the presence of higher percentage of nickel content led to the enhancement in ductility and impact toughness properties. On the other hand, the formation of fully ferritic structure in the weld metal region of GMAFSS joint due to the presence of higher percentage of chromium and carbon (very less percentage of nickel) content led to the reduction in ductility and impact toughness properties. However, the formation of combined ferritic and austenitic structure in the weld metal region of GMADSS joint due to the presence of balanced percentage of chromium, nickel, and molybdenum content led to the higher strength and hardness properties.

Higher yield strength and tensile strength of the GMADSS joint are greatly used to enhance the endurance limit of the joints, and hence the FCI is delayed. The combined effect of higher yield strength and relatively higher toughness compared to base metal of the GMADSS joint offers enhanced resistance to crack initiation and crack propagation, and hence the fatigue performance of the joints is superior as compared to their counterparts.

The crack growth exponent m, which is derived from the relationship existing between crack growth rate (da/dN) and SIF range, is an important parameter to evaluate the fatigue crack growth behavior of materials since it decides the FCP life of the materials. This exponent is obtained from the slope of the curve drawn between da/dN and SIF range. If this exponent is lower, then the slope of the curve is lower, indicating that the resistance offered by the material to the growing fatigue crack is higher and hence the fatigue life will be longer. If this exponent is larger, then slope of the curve is higher, indicating that the resistance offered by the material to the growing fatigue crack is lower and hence the fatigue life will be shorter (Ref 13). The crack growth exponent m for GMADSS joint is lower compared to GMAFSS and GMAASS joints (Table 4), and this indicates that the GMADSS joint offers higher resistance to fatigue crack growth compared to GMAFSS and GMAASS joints.

Slope of the S-N curve is another measure to understand the fatigue performance of welded joints. If the slope of the S-N curve is larger, then the fatigue life will be higher and vice versa. The slope of S-N curve is larger for GMADSS joint as compared to GMAFSS and GMAASS joints (Fig. 5).

In the lower ductility and toughness weld metal, as in the case of GMAFSS joints, since the deformation and the yield are mainly concentrated in the weld metal region, the extension of the plastic zone is limited within the fusion zone (Ref 14). The triaxial state of stress is high in WM region and the relaxation of this stress is poor. The crack driving force needed for crack extension is small. So, the fracture toughness of the lower ductility weld metal is not high. On the other hand, if strength of the weld metal is higher, the stress relaxation can easily take place in the crack tip region. So more crack driving force is needed for crack extension, and the fracture resistance of the high strength weld metal region is greater than that of the low strength weld metal region (Ref 15). This is also one of the reasons for better fatigue resistance of the GMADSS joints.

5. Conclusions

From this investigation, following important conclusions are derived:

- The FCI behavior, FCP behavior, and fatigue life of FSS joints fabricated using DSS filler metal are superior

compared to the joints fabricated using ASS and FSS filler metals.

- GMADSS joints endured 20% higher number of cycles compared to GMAASS joints and 40% higher number of cycles compared to GMAFSS joints.
- The combined effect of higher yield strength and relatively higher toughness of the GMADSS weld metal offers enhanced resistance to crack initiation and crack propagation, and hence the fatigue performance of the joints is superior as compared to their counterparts.

Acknowledgments

References

1. P. Sathiya, S. Aravindan, and A. Noorul Haq, Effect of Friction Welding Parameters on Mechanical and Metallurgical Properties of Ferritic Stainless Steel, *Int. J. Adv. Manuf. Technol.*, 2007, **31**, p 1076–1082

2. F.B. Pickering, Physical Metallurgy of Stainless Steel Developments, *Int. Met. Rev.*, 1976, **21**, p 227–268

3. S. Kou, *Welding Metallurgy*, Wiley, New York, 1987, p 383–386

4. E. Folkhard, *Welding Metallurgy of Stainless Steels*, Spring-Verlag Wien, New York, 1988

5. J.C. Villafuerte and H.W. Kerr, Grain Structures in Gas Tungsten Arc Welds of Austenitic Stainless Steels with Ferrite Primary Phase, *Metall. Trans. A*, 1990, **21A**, p 979–986

6. J.C. Villafuerte, H.W. Kerr, and S.A. David, Mechanisms of Equiaxed Grain Formation in Ferritic Stainless Steel Gas Tungsten Arc Welds, *Mater. Sci. Eng.*, 1995, **194**, p 187–191

7. T. Mohandas, G. Madhusudhan Reddy, and M. Naveed, A Comparative Evaluation of Gas Tungsten and Shielded Metal Arc Welds of a "Ferritic" Stainless Steel, *J. Mater. Process. Technol.*, 1999, **94**, p 133–140

8. A.M. Meyers and M. du Toit, Interstitial Diffusion of Carbon and Nitrogen into Heat Affected Zones of 11–12% Chromium Steel Welds, *Weld. Res. Suppl.*, 2001, **80**, p 275-s–280-s

9. C.C. Silva, J.P. Farias, H.C. Miranda, R.F. Guimaraes, J.W.A. Menezes, and M.A.M. Neto, Microstructural Characterization of the HAZ in AISI 444 Ferritic Stainless Steel Welds, *Mater. Charact.*, 2008, **59**(5), p 528–536

10. S. Ravi, V. Balasubramanian, and S. Nemat Nasser, Effect of Notch Location on Fatigue Crack Growth Behavior of Strength-Mismatched High-Strength Low-Alloy Steel Weldments, *J. Mater. Eng. Perform.*, 2004, **13**, p 758–765

11. S. Ravi, V. Balasubramanian, and S. Nemat Nasser, Fatigue Life Prediction of Strength Mis-matched High Strength Low Alloy Steel Welds, *Mater. Des.*, 2006, **27**, p 278–286

12. B. Guha, A New Fracture Mechanics Method to Predict the Fatigue Life of Welded Cruciform Joints, *Eng. Fract. Mech.*, 1995, **52**, p 215

13. C.S. Kusko, J.N. Dupont, and A.R. Marder, Fatigue Crack Propagation of Stainless Steel Welds, *International Trends in Welding Research of Conference Proceedings*, 2002, p 70

14. H. Mayer, M. Papakyriacou, R. Pippen, and S. Stanzl-Tschegg, Influence of Loading Frequency on the High Cycle Fatigue Properties of Al-Zn-Mg-Cu 1.5 Aluminium Alloy, *Mater. Sci. Eng.*, 2001, **314**, p 48–54

15. G. Madhusudhan Reddy, A.A. Gokhale, and K. Prasad Rao, Optimization of Pulse Frequency in Pulsed Current Gas Tungsten Arc Welding of Aluminium-Lithium Alloy Sheets, *J. Mater. Sci. Technol.*, 1998, **14**, p 61–68